Journal of Fluorine Chemistry 144 (2012) 10–16

Contents lists available at SciVerse ScienceDirect

Journal of Fluorine Chemistry

journal homepage: www.elsevier.com/locate/fluor

Tribological properties of fluorinated nanocarbons with different shape factors

N. Nomède-Martyr [a,b,c], E. Disa [a,b], P. Thomas [c], L. Romana [c], Jean-Louis Mansot [c,d,**], M. Dubois [a,b,*], K. Guérin [a,b], W. Zhang [a,b,e], A. Hamwi [a,b]

[a] Clermont Université, Université Blaise Pascal, Institut de Chimie de Clermont-Ferrand (ICCF, UMR 6296), Inorganic Materials team, 63171 Aubière, France
[b] CNRS, UMR 6296, 63170 Aubière, France
[c] Groupe de Technologie des Surfaces et Interfaces (GTSI, EA 2432), Faculté des Sciences Exactes et Naturelles, Université des Antilles et de la Guyane, 97159 Pointe à Pitre Cedex, France
[d] Centre Commun de Caractérisation des Matériaux des Antilles et de la Guyane (C^3MAG), Faculté des Sciences Exactes et Naturelles, Université des Antilles et de la Guyane, 97159 Pointe à Pitre Cedex, France
[e] Ecole Centrale de Pékin, Beijing University of Aeronautics and Astronautics (BUAA), Road 37, HaiDian District, Beijing 100191, China

ARTICLE INFO

Article history:
Received 22 July 2012
Received in revised form 26 August 2012
Accepted 27 August 2012
Available online 18 September 2012

Keywords:
Fluorination
Nanolubricant
Nanocarbon
Friction
Tribology

ABSTRACT

The structural parameters of fluorinated nanocarbons presenting different shapes, i.e. spherical, tubular and discotic are investigated and correlated to their tribological properties. Different fluorination rates of graphitized carbon blacks (0D), carbon nanofibres (1D) and a mixture of carbon nanodiscs and nanocones (2D) were achieved under pure molecular fluorine gas flow (direct fluorination). Raman spectrometry, X-ray diffraction and ^{19}F solid state nuclear magnetic resonance underline similar structure and nature of the C–F bonds (covalent) for equivalent fluorine contents. In spite of the similarities of physical–chemical properties at equivalent fluorine contents, the tribological properties of the fluorinated nanocarbons differ. Those properties are discussed taking into account the role of the fluorine content and location of the fluorine atoms in the decrease of the interparticle interactions and in the cleavage of the external fluorocarbon layers to form the tribofilm. Finally, the effect of the shape is discussed.

1. Introduction

During the last three decades, the increase of severity of lubrication conditions in engines and environment protection purpose are at the origin of the development of new additivation strategies for lubrication in the boundary regime. These developments are mainly investigated to overcome the insufficiency of conventional lubricant additives which protective efficiency depends on their reactivity with the sliding surfaces, associated to the occurrence of formation of a protective tribofilm and which present high sulfur and phosphorus contents [1–4]. These new strategies of lubrication consist in the introduction of either solid nanoparticles of tribo-active phases [2] or precursor of tribo-active phases [3,4] in the lubricant base. These new nano-additives are subjected to form the protective tribofilm, in the physical–chemical conditions of a sliding boundary contact, without any chemical reactions with the sliding surfaces. Nano-particles of lamellar compounds or precursors of lamellar compounds such as carbonaceous nanomaterials (carbon nanotubes, onions, nano-horns, peapods…) are promising candidates as far as carbon lamellar compounds (graphite) already present good intrinsic friction properties [1,5]. These good properties are associated to the layered structure of graphite type phases where graphene layers are separated by van der Waals gaps through which interactions between graphene layers are extremely weak [6]. Previous studies also showed that the tribological properties of graphite strongly depend on the environmental conditions [7–10] which are able to significantly modify the surface energy of the particles and then the interparticular interactions leading in many cases to an improvement of the intrinsic properties recorded under vacuum or in dry air.

In the present work two strategies are investigated to improve the tribological properties of nanocarbon phases [11–13]:

- The modification of nanoparticle surface energies by chemical covalent functionalization with fluorine atoms.
- The optimization of the shape/dimensional factors (spherical = 0D, cylindrical = 1D, discotic = 2D).

The friction properties of the pristine carbon nanophases and fluorinated ones obtained via the two strategies are investigated in

* Corresponding author at: Clermont Université, Université Blaise Pascal, Institut de Chimie de Clermont-Ferrand (ICCF, UMR 6296), Inorganic Materials team, 63171 Aubière, France. Tel.: +33 473407105; fax: +33 473407933.
** Corresponding author at: Groupe de Technologie des Surfaces et Interfaces (GTSI, EA 2432), Faculté des Sciences Exactes et Naturelles, Université des Antilles et de la Guyane, 97159 Pointe à Pitre Cedex, France. Tel.: +33 590483097.
E-mail addresses: jean-louis.mansot@univ-ag.fr (J.-L. Mansot), Marc.DUBOIS@univ-bpclermont.fr (M. Dubois).

0022-1139/$ – see front matter © 2012 Elsevier B.V. All rights reserved.
http://dx.doi.org/10.1016/j.jfluchem.2012.08.008

order to evaluate the influence and benefits associated to each structural/chemical parameters.

0D materials (spherical carbon blacks), 1D nanocarbons (carbon nanofibres) and 2D ones (carbon nanodiscs) with similar crystalline order (graphitized materials) were selected and fluorinated using molecular fluorine F_2. The tribological properties of the resulting derivatives were then investigated. As a matter of fact, the C–F bonding is highly versatile in fluorinated carbons. The nature of the interactions between the fluorine and the carbon atoms can considerably vary: in the case of the fluorine adsorption on the surface of carbonaceous materials, these interactions are very weak. On the other hand, a covalent, semi-ionic or ionic character can be obtained [14,15]. In particular, intermediate states are observed in compounds where fluorinated carbon atoms, with sp^3 hybridization, and non-fluorinated sp^2 ones coexist in the layers (hyperconjugation) [16,17]. The nature of the C–F bonds depends on the synthesis conditions; for covalent compounds, namely graphite fluorides $(C_2F)_n$ and $(CF)_n$, prepared with molecular fluorine at 350 °C and 600 °C [17,18], respectively, the carbon skeleton consists of trans-linked cyclohexane chairs or cis-trans linked cyclohexane boats with sp^3 hybridization. In the case of fluorine–graphite intercalation compounds (C_xF), obtained at temperature lower than 100 °C, the planar configuration of graphite is partially preserved; the nature of the C–F bond evolves from ionic for low fluorine contents to covalent for higher fluorine contents. Moreover, due to the high number of walls, the curvature of nanofibres is low and does not affect the C–F bonding contrary to the cases of single, double or low diameter multiwalled nanotubes or fullerenes [19].

In the first part of the present paper, the physical–chemical characterization of the fluorinated carbons using ^{19}F solid state nuclear magnetic resonance (NMR), X-ray diffraction (XRD) and Raman spectroscopy will be discussed in order to underline the structural order and the nature of the C–F bonds. The tribological properties will be then compared for the 0D, 1D and 2D fluorinated nanocarbons.

2. Experimental

2.1. Carbonaceous nanomaterials

The 0D compounds were prepared from carbon blacks provided by Superior Graphite, graphitized by high temperature treatment (2000 °C under argon) and denoted as GCBs in the paper. Transmission electron microscopy (TEM) showed for the same commercial product that highly graphitized layers surround the core of the particles; this outer shell of about 10 nm thickness results from the graphitization process [20].

The 1D materials were synthesized from high purity (>90%) carbon nanofibres (CNFs), of 2–20 microns length, supplied by MER Corporation, Tucson, Arizona. They were obtained by chemical vapor deposition (CVD) and heat treated at 1800 °C in an argon atmosphere to enhance their graphitization degree.

The 2D samples consist in a mixture of carbon nanodiscs (70 weight %), carbon nanocones (20 weight %) and amorphous carbon (10 weight %), provided by NTec Norway [21,22] annealed under argon at 2700 °C for graphitization. Because of the large amount of discs, the mixture will be denoted CNDs. CNDs were produced by pyrolysis of heavy oil using the Kvaerner Carbon Black and Hydrogen Process (CBH) [23].

2.2. Fluorination conditions

Direct fluorination was carried out with pure fluorine gas flow in a Monel reactor. Different fluorine contents were obtained according to the fluorination temperatures T_F with constant duration of 3 h and F_2 gas flux of 10 mL min^{-1}. The fluorine content "x" of the fluorinated nanocarbons, expressed as the atomic F/C ratio, was determined first by gravimetry upon fluorination (weight uptake method) and confirmed by quantitative ^{19}F NMR analyses. Details on synthesis and direct fluorination mechanism have been already published elsewhere [22,24]. Four different fluorine contents for every fluorinated carbons were selected close to x = 0.15, 0.65, 0.75 and 1. The accuracy of F/C is ±0.02.

Carbon nanofibres were placed under a pure fluorine gas flow (1 atm) at temperatures T_F ranging between 405 and 480 °C; the resulting samples are denoted CNF-T_F. Fluorinated carbon nanodiscs were obtained at temperatures ranging between 450 and 520 °C (CND-T_F). For graphitized carbon blacks, three samples were obtained by fluorination in the 360–410 °C range for 3 h, the highest fluorination rate (F/C = 1.04) being prepared at 400 °C for 48 h. The resulting samples are called GCB-T_F.

2.3. Physical–chemical characterizations

^{19}F NMR experiments were carried out using a Bruker Avance spectrometer, with a working frequency of 282.2 MHz. A magic angle spinning (MAS) probe (Bruker) operating with a 4 mm rotor was used. For MAS experiments, a simple sequence was performed with a single $\pi/2$ pulse length of 4.0 μs. ^{19}F chemical shifts were externally referenced to $CFCl_3$. To confirm the molar ratio F/C obtained by weight uptake method, quantitative ^{19}F NMR measurements were carried out using the same conditions for each sample, i.e. similar receiver gain, scan number and recycling time D_1 ($D_1 > 5T_1$ where T_1 is the spin–lattice relaxation time T_1, usually $T_1 < 500$ ms in air [25,26] so D_1 was equal to 3 s). The intensities are divided by the sample mass. Polyvinyldifluoride $(CF_2–CH_2)_n$ was used as a standard for the fluorine content quantification.

Secondary electron images were recorded on a ZEISS Supra 55VP Scanning electron microscopy (SEM) operating in high vacuum at accelerating voltage between 4 and 15 kV, using an Everhart–Thornley detector. Specimens were prepared by sticking powder on the surface of an adhesive carbon film.

X-ray diffraction diagrams were obtained using a X Pert Pro Philips diffractometer with a Cu anode (Cu Kα radiation, λ = 1.5406 Å).

Raman spectrometry was performed at room temperature using a Jobin Yvon T64000 with a charge coupled device multichannel detector. The excitation light was the 514.5 nm wavelength line delivered by an Argon ion laser. The laser power was tuned at 10 mW.

The tribological properties of the nanocarbons were evaluated using a ball-on-plane reciprocal tribometer consisting of an AISI 52100 steel ball rubbing against an AISI 52100 steel plane. The surfaces were polished in order to obtain roughness of the ball and the plane of 20 nm and 200 nm RMS, respectively. The high roughness of the plane is needed to improve the adhesion of the tested materials which were deposited onto the plane by a burnishing method; the latter consists of the crushing of nanomaterial powder between two planes leading to surface films of thicknesses in the 1–3 μm range. The sliding speed of the ball on the plane was 6 mm s^{-1} and the normal applied load F_N of 10 N leaded to a contact area with a diameter of 140 μm and a mean contact pressure of 0.65 GPa (according to Hertz theory). The tangential force F_T was measured with a computer-based data acquisition system. The friction coefficient is defined as $\mu = F_T/F_N$.

At the beginning of the tribological experiment, when the loaded sphere on plane contact was established, one drop of pentane (boiling point of 36 °C) was added in order to improve the feeding of the sliding contact with nanoparticles and then to

facilitate the formation of the tribofilm. The friction coefficients obtained just after pentane evaporation were considered to correspond to the intrinsic tribologic properties in air of the various fluorinated nanocarbons. Their evolutions, as a function of the cycles number, were also studied by means of long term experiments.

3. Results and discussion

3.1. Physical–chemical characterization

Fig. 1 presents secondary electrons micrographs recorded by scanning electron microscopy on the three initial compounds used as precursors for the syntheses of the fluorine derivatives.

The 0D character of the graphitized carbon blacks is emphasized by the spherical shape of the nano particles with average diameter of 44 nm (Fig. 1a). Moreover, GCBs mainly consist in aggregated spherical particles. Their specific surface area (SSA) was found equal to 46 $m^2\ g^{-1}$ [20].

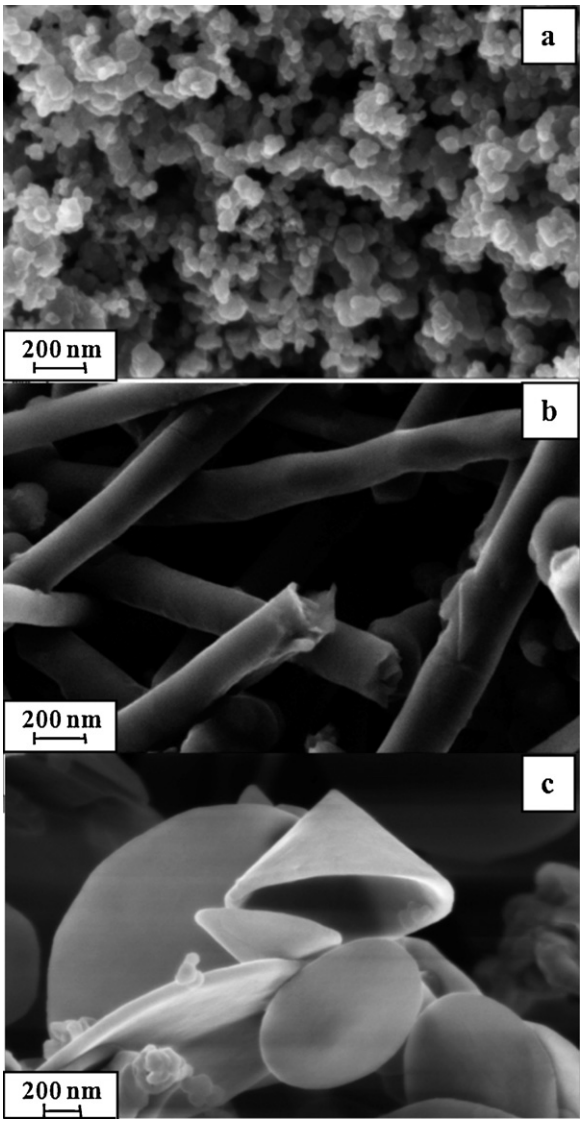

Fig. 1. SEM images of the highly fluorinated nanocarbons with F/C ~ 1: (a) graphitized carbon blacks consist in spherical particles (0D), (b) carbon nanofibres consist in concentric cylinders of graphite sheets or single graphite sheet rolled in around itself (1D) and (c) a mixture of carbon nanodiscs and nanocones are formed by conical/discotic graphene stacking (2D).

Table 1
The resulting fluorination F/C determined by quantitative ^{19}F NMR measurements.

GCBs		CNFs		CNDs	
Temperature (°C)	F/C	Temperature (°C)	F/C	Temperature (°C)	F/C
360	0.16	405	0.15	450	0.14
380	0.69	428	0.59	480	0.62
410	0.78	450	0.72	500	0.75
400 (2 days)	1.04	480	1.04	520	1

The morphology of the carbon nanofibres (Fig. 1c) characterized by quite cylindrical shapes with diameters in the 100–200 nm range and length in the 5–10 μm range (Fig. 1b) points out the 1D character of these compounds. SSA of these fibres is equal to 19 $m^2\ g^{-1}$ [25].

The micrograph collected on 2D material shows flat particles presenting nanodiscs and nanocones shapes with diameters ranging from 0.8 to 3.2 μm and 0.5 to 2.8 μm, respectively, and typical thicknesses lying in the 15–65 nm range. Cones exhibit different apex angles equal to 112.9°, 83.6°, 60.0°, 38.9° and 19.2° [21,23]. SSA of CNDs is equal to 29 $m^2\ g^{-1}$.

Due to the various reactivities of the initial carbonaceous phases with fluorine gas that strongly depend on their structure and morphology, different reaction temperatures were used to obtain the target F/C ratio needed for the comparative study. These reaction temperatures are summarized in Table 1 with the effective F/C ratios determined by quantitative ^{19}F NMR spectrometry. Fluorination needs both the change of the carbon hybridization from sp^2 to sp^3 and accommodation of the fluorine atoms that results in drastic volume expansion. Atomic force microscopy underlines that highly fluorinated nanodiscs were swelled without cracks because of the accommodation of fluorine atoms [22]. The swelling was more pronounced on the edges and the maximum swelling was observed in the overall perimeter. The edge seems then to be the preferential pathway of fluorine atoms/molecules for the fluorination. For carbon blacks and nanofibres, the structures are closed and the fluorine diffusion started in sheet defects. The small size of the graphitized carbon blacks particles associated with their high defect density, induced by the geometric constraints of the graphene layers, let suppose a high reactivity of this material with fluorine. As a consequence, the fluorination temperature is quite low because of relatively easy diffusion of fluorine in the structure.

Previous works [24] allow us to demonstrate that for carbon nanofibres, the first steps of their direct fluorination result essentially in fluorination of the external (surfacic) graphene layers. When the fluorination temperature increases, fluorination progresses towards the inner layers of the nanostructure.

Higher fluorination temperatures are needed for nanodiscs as far as sheet edges are the starting points of the fluorination and that fluorine atoms must diffuse in the interlayer van der Waals gap.

The XRD diagrams collected on the different initial compounds and their fluorinated derivatives are presented in Fig. 2.

The diagrams of the initial nanocarbon phases present an intense peak around 26° assigned to the (0 0 2) graphite reflection which corresponds to the graphene interlayers distances equal to 0.34 nm for every materials (discs, fibres and carbon blacks). The coherence length along the *c* axis L_c was estimated from the width of the (0 0 2) peak according to Scherrer's formula. The L_c values reported in Table 2 are 7, 13 and 43 nm for raw GCBs, CNFs, and CNDs, respectively. The progressive decrease of the (0 0 2) peak intensity as a function of the fluorination temperature T_F for all compounds allow us to follow structural changes induced by the progression of the fluorination process. It is surprising to note that

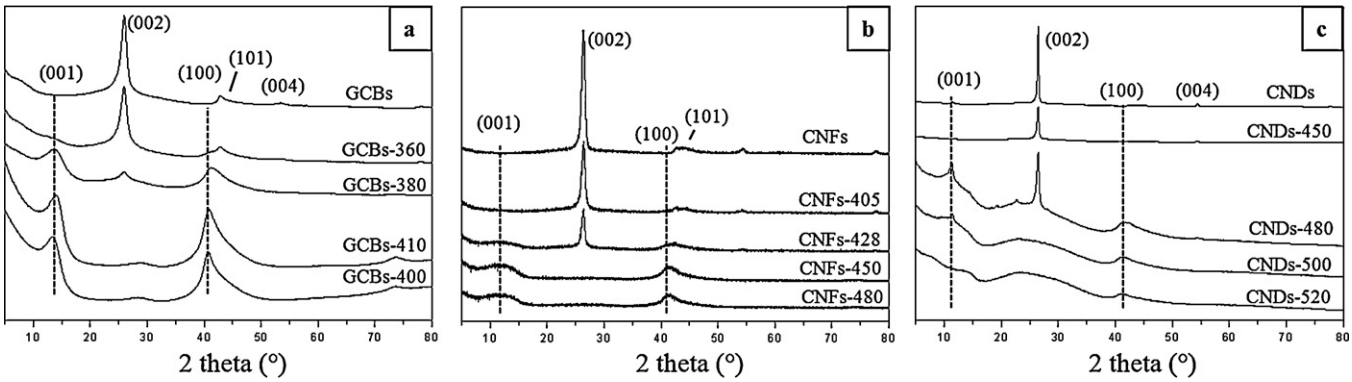

Fig. 2. XRD patterns of the different fluorinated and starting nanocarbons: (a) graphitized carbon blacks GCBs, (b) carbon nanofibres CNFs and (c) carbon nanodiscs CNDs.

the (0 0 2) peak completely disappears for similar fluorine contents (around 0.75) whatever were the initial carbon phases, its morphology and the fluorination temperature needed (410, 450 and 500 °C for GCBs (F/C = 0.78), CNFs (F/C = 0.72) and CNDs (F/C = 0.75), respectively).

The formation of the fluorinated phases is underlined by the appearance of new peaks in the X-ray diffractograms corresponding to the (0 0 1) and (1 0 0) inter reticular distances of a fluorinated phase in an hexagonal structure. In the case of the GCBs, an enlarged peak appears at 14.5°, corresponding to the 0.6 nm inter reticular distance characteristic of the $(CF)_n$ type structure formation [15], which intensity increases with reaction temperature. In the case of CNDs, a narrow peak appears at 11.3° corresponding to a 0.76 nm inter reticular distance close to the $(C_2F)_n$ for reaction temperature under 500 °C. A shoulder at 14.5° (0.6 nm) increasing with temperature shows the formation of the $(CF)_n$ phase which is the only one present for the reaction temperature of 520 °C. The appearance of an enlarged peak at around 13° in the diffractograms of the CNFs seems to indicate the presence of a mixture of $(CF)_n$ and $(C_2F)_n$ phases whatever the fluorination temperature.

The enlarged peaks corresponding to (0 0 1) and (1 0 0) inter reticular distances clearly point out that the fluorination process introduces structural disorder and consequently a reduction of the crystallized domains sizes expressed as the coherence length L_c perpendicular to the layers. The L_c values calculated from either (0 0 2) diffraction peak of graphite or (0 0 1) peak of the fluorinated phase (set in italic in the table) for the various nanocarbons are summarized in Table 2. As the fluorine content increases, the average mono crystalline domain size decreases. The decrease of the coherence length is more important for the fluorinated nanofibres ($L_{c\text{-initial}}$ = 13 nm to $L_{c\text{-F/C=1}}$ = 9 nm) and nanodiscs ($L_{c\text{-initial}}$ = 43 nm to $L_{c\text{-F/C=1}}$ = 15 nm) than in the case of fluorinated GCBs ($L_{c\text{-initial}}$ = 7 nm to $L_{c\text{-F/C=1}}$ = 5 nm). This can be explained by the lower initial value for graphitized carbon blacks.

Structural information about the extension of the graphitic monocrystalline domains perpendicularly to the *c* axis were investigated by Raman spectrometry. Because the C–F vibration is not active in Raman, this technique focuses on the non-fluorinated carbon lattice, which could be however affected by the neighbouring fluorinated parts. The Raman spectra collected on the various fluorinated compounds are presented in Fig. 3. Most of the spectra present three bands as classically observed for carbonaceous materials. The vibration band at 1580 cm^{-1} corresponds to the well known G band characteristic of graphite structure. The two bands near 1345 cm^{-1} and 1620 cm^{-1} are assigned to the *D* and *D*' modes and appear when disorder is present in the graphitic lattice, characterizing the impurities and/or defects. In all fluorinated families, the *D* and *D*' bands relative intensities increase as a function of the fluorination temperatures showing a size reduction of the remaining graphitic domains. The *D* band downshift also recorded in the three families is attributed both to size reduction of the graphitic domains and to the creation of covalent C–F bonds [10,28,29,30]. It is to note that the presence of G and D bands for CNDs-520 highlights that the sample contains unreacted sp^2 carbon atoms although F/C equal to 1 (Table 1). As revealed by NMR, CF_2 and CF_3 groups are present; the chemical composition CF_x is better written $C_{1-y-z-w}(CF)_y(CF_2)_z(CF_3)_w$ with $x = y + 2z + 3w$. With this notation, non-fluorinated carbon atoms are underlined.

The size reduction of the remaining graphitic domains in the fluorinated compounds is expressed as the coherence length L_a corresponding to their spatial extension perpendicular to the *c* axis. The L_a values deduced from the I_D/I_G intensity ratios using the formula $L_a = C(\lambda)/(I_D/I_G)$, where $C(\lambda) = C_0 + \lambda C_1$ is equal to 10.3 nm with an excitation wavelength of 514.5 nm, C_0 and C_1 are nearly constant in the 400–700 nm wavelength range (C_0 = 12.6 nm and C_1 = 0.033 nm) [31], are reported in Table 2. The decrease of the spatial extension of the graphitic domains from initial carbon phases to fluorinated derivatives highlights the progressive conversion of the graphite lattice into fluorinated phases.

^{19}F MAS NMR spectra recorded on the various fluorinated compounds with spinning speed of 14 kHz are shown in Fig. 4. A similar value of the ^{19}F chemical shift (−190 ppm/$CFCl_3$) of the main line is observed for all the compounds whatever the fluorination contents. These results indicate that the nature of the C–F bonds is covalent in all fluorinated derivatives [18,25–27]. The presence of an isotropic line at −130 ppm indicates the presence of some CF_2 groups. CF_2 contents are generally well correlated with the amount of CF_3 groups. For each spectrum of nanocarbons, narrow lines are present in the −60/−90 ppm range corresponding to CF_3 groups and are superimposed with spinning sidebands of C–F and CF_2 lines. The intensity of the lines related to the amounts of CF_2 and CF_3 groups is equivalent for compounds presenting similar fluorine content whatever the precursor.

As a conclusion on this first set of results, the fluorination of 0D, 1D and 2D nanocarbons results in fluorinated compounds presenting similar C–F bonds and nanostructuration whereas

Table 2
Calculated coherence lengths by XRD analysis (L_c) and by Raman spectroscopy (L_a).

F/C	GCBs		CNFs		CNDs	
	L_c (nm)	L_a (nm)	L_c (nm)	L_a (nm)	L_c (nm)	L_a (nm)
0	7	7	13	16	43	38
~0.15	6	4	13	9	27	9
~0.65	5	2	15	3	20	1.2
~0.75	*5*	*4*	*9*	*2.5*	*15*	*2*
~1	*5*	*4*	*9*	*Fluorescence*	–	*1.5*

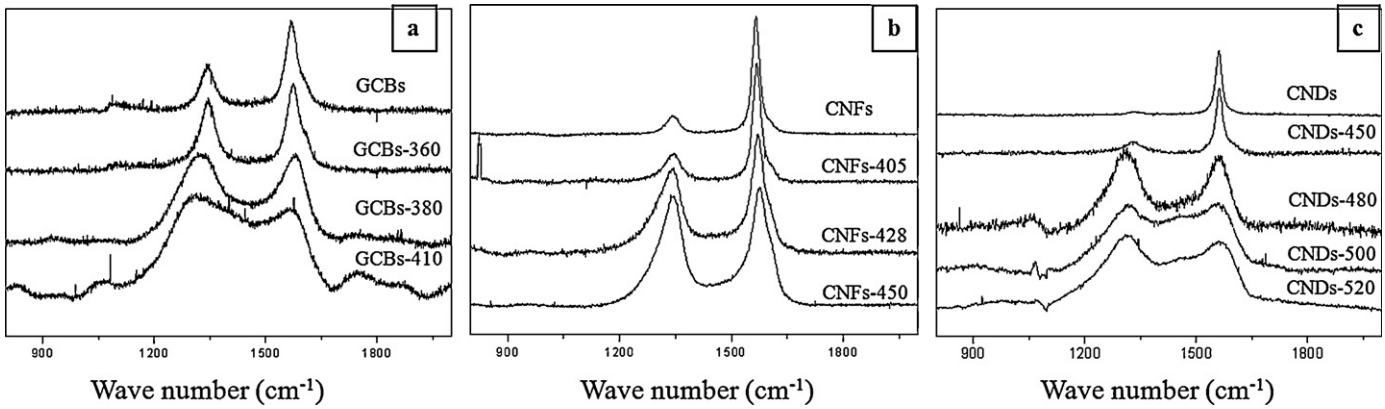

Fig. 3. Raman spectra of the different fluorinated nanocarbons: (a) graphitized carbon blacks GCBs, (b) carbon nanofibres CNFs and (c) carbon nanodiscs CNDs. Because of the strong fluorescence, the spectra of GCBs-400 and CNFs-480 were not obtained.

structural differences were observed for initial materials. This is related to the conversion of the carbon hybridization from sp^2 to sp^3 and the structural changes from graphite into fluorinated phases either $(CF)_n$ or a $(C_2F)_n/(CF)_n$ mixture. For a given fluorine content, the structural parameters L_a and L_c are quite similar. As an example, L_c values are 7, 13 and 43 nm for initial GCBs, CNFs and CNDs, respectively. When F/C is 0.75, the L_c values are 5, 9 and 15 nm for GCBs-410, CNFs-450 and CNDs-500, respectively.

3.2. Tribological properties

As already mentioned in Section 2, the tribological experiments start in the presence of pentane in order to establish a stable and compact film of nanoparticles on the sliding surfaces without significant changes of the nanoparticles structures and morphologies [12]. The evaporation of the liquid allows us to determine the intrinsic friction coefficient of the materials in air. As a typical example of the tribological behaviour of the various fluorinated derivatives, Fig. 5 presents the evolution of the friction coefficient of fluorinated nanofibres (F/C = 0.72). In the presence of pentane, the friction coefficient was around 0.06. This value remained stable as long as the pentane is present. As shown in previous studies the friction reduction recorded in the presence of pentane is attributed to the simultaneous presence of the solid particles and the organic liquid in the sliding contact. During pentane evaporation the friction coefficient increased and raised the intrinsic value of the tested compound here 0.08 after complete evaporation of the liquid. The friction coefficients obtained for all studied compounds are reported in Table 3. It can be first noticed that the friction coefficients of the non-fluorinated nanocarbons

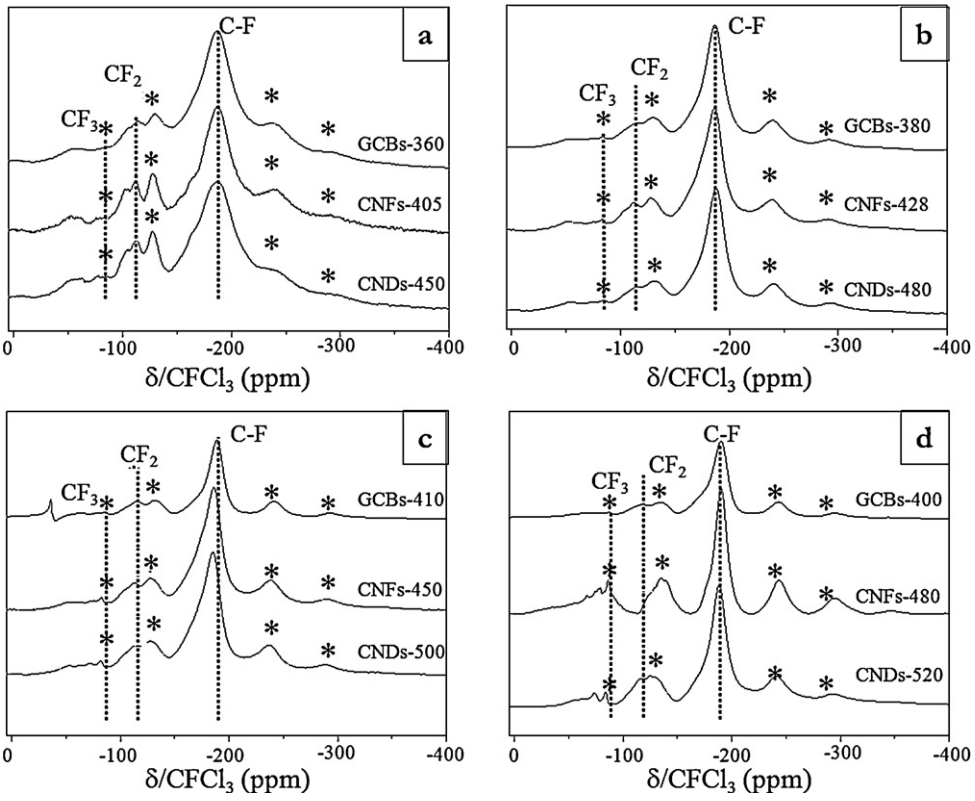

Fig. 4. ^{19}F NMR spectra of the fluorinated nanocarbons: (a) with F/C ~ 0.15, (b) with F/C ~ 0.65, (c) with F/C ~ 0.75 and (d) with F/C ~ 1.

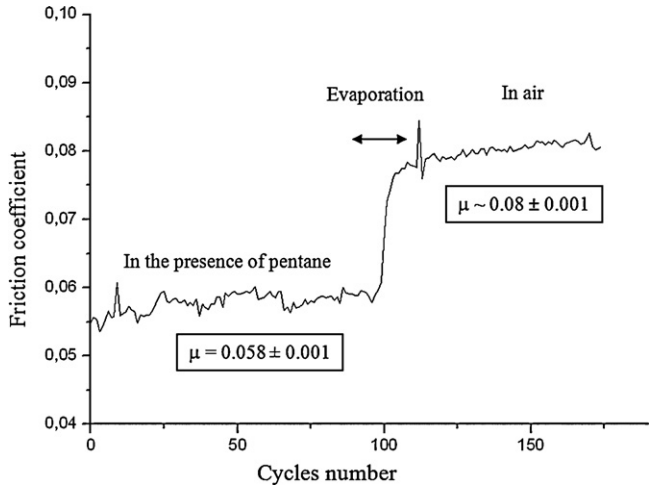

Fig. 5. Evolution of the friction coefficient of CNF-480 according to cycles number. The tribological test starts in the presence of pentane in order to improve the establishment of the tribofilm. The intrinsic coefficient is measured during the stable phase after pentane evaporation $\mu_{CNFs\text{-}480} = 0.08$ in air.

differ significantly in comparison with the fluorinated ones. For the cases of graphitized carbon blacks ($\mu_{GCBs} = 0.12 \pm 0.01$) and carbon nanofibres ($\mu_{CNFs} = 0.14 \pm 0.01$), the friction coefficients are close to those obtained for graphite in air (0.10–0.15) whereas μ is lower ($\mu_{CNDs} = 0.08 \pm 0.01$) for the graphitized nanodiscs. This can be attributed to the highly organized structure of CNDs (large graphitic domains) compared to the other nanocarbons [13]. The fluorination process leads to an improvement of the friction properties (decrease of the friction coefficient) for CNFs and GCBs ($0.065 < \mu < 0.085$) whereas the friction coefficient recorded in the case of CNDs remains constant whatever the F/C content.

Using the freeze fracturing technique, Naess et al. [21] observed for the non-graphitized nanodiscs from N-Tec, an in-plane cleavage that usually was parallel to the disc surface. The particles were fractured in a plane close to the geometrical centre of the disc. The splitting occurs between the graphitic layers, which are only bonded by weak van der Waals forces, and not in the amorphous carbon surrounding the disc parts. The authors concluded then that the as-synthesized discs can be described as a graphitic core within an envelope of ill organized carbons; The graphitic core (2–5 nm thickness) being first grown up to the final diameter of the nanodiscs, the deposition of amorphous carbon on the initial graphitic core leads to the final thickness. The heat-treatment at 2700 °C induces the graphitization of the ill organized carbon parts with a growth of the graphitic domains parallel to the initial graphitic core (parallel to the disc surfaces) as already demonstrated by AFM measurements [13,22]. This extended graphitic structure may result in the reduction of friction through cleavage between the graphene layers. The flat (2D) morphology with large diameter/thickness ratio strongly induces an orientation of the nanodiscs parallel to the sliding surfaces. Their extended graphitic structure with *c* axis perpendicular to disc faces seems to induce easy cleavage along sliding directions parallel to the disc surfaces. This combination of orientation in the tribological interface and mechanical behaviour appears to be at the origin of the exceptional friction reduction properties. As a consequence, the fluorination

Table 3
The intrinsic friction coefficients of the fluorinated nanocarbons measured in air.

F/C	Friction coefficients		
	GCBs	CNFs	CNDs
0	0.12 ± 0.001	0.14 ± 0.02	0.08 ± 0.01
~0.15	0.075 ± 0.001	0.085 ± 0.001	0.075 ± 0.015
~0.65	0.065 ± 0.001	0.075 ± 0.001	0.085 ± 0.005
~0.75	0.070 ± 0.001	0.080 ± 0.001	0.080 ± 0.005
~1	0.070 ± 0.001	0.080 ± 0.001	0.095 ± 0.005

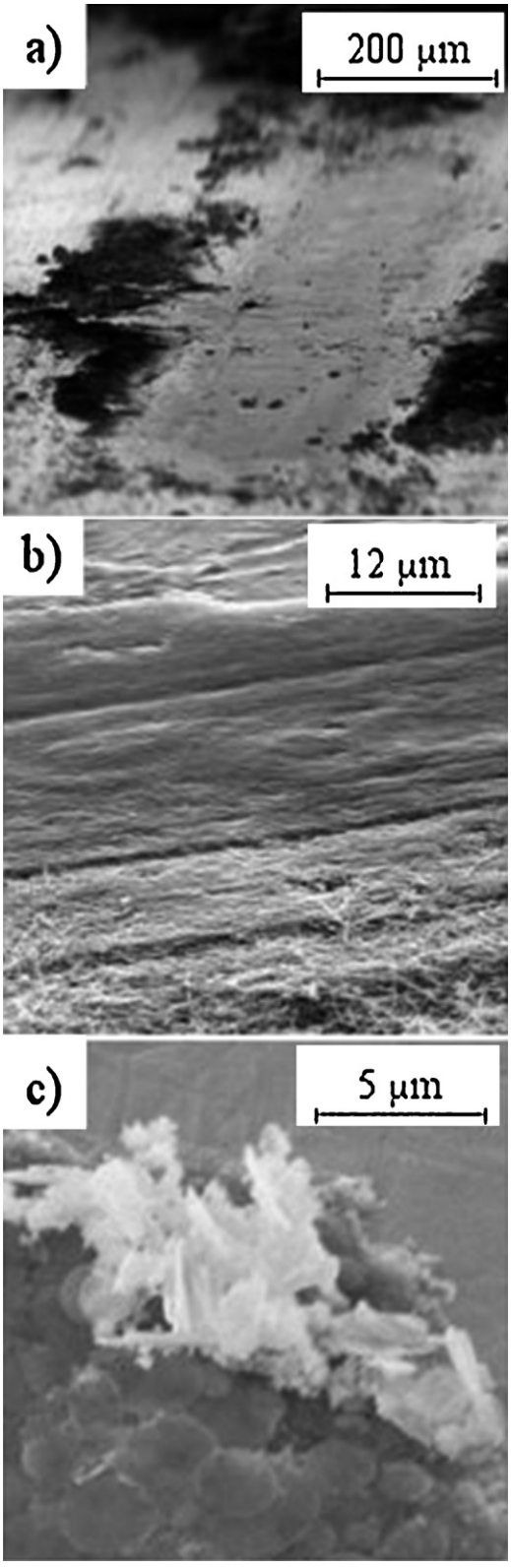

Fig. 6. SEM micrographs showing the aspect of the tribofilms for fluorinated nanocarbons: (a) graphitized carbon blacks GCBs, (b) carbon nanofibres CNFs and (c) carbon nanodiscs CNDs.

process does not induce any significant changes compared to the friction properties of the initial graphitized compound.

At a given fluorination level, the friction coefficients of the graphitized carbon blacks are lower than for CNDs. This difference is clearly visible for the highest fluorine content (F/C = 1) as $\mu_{GCBs\text{-}400} = 0.070$, $\mu_{CNFs\text{-}480} = 0.080$ and $\mu_{CNDs\text{-}520} = 0.095$. Because the fluorinated nanocarbons present similar structures and C–F bonding, an effect of the shape factor of the fluorinated nanocarbons on the tribological properties can be proposed.

Due to their structure and shape factor (diameter/thickness ratio) the CNDs appear as a particular case. The cleavage is facilitated even in the non-fluorinated sample contrarily to both CNFs and GCBs for which the presence of fluorine atoms, within the interlayer spacing, significantly enhances the cleavage. Moreover, the nanostructuration with either concentric cylinders of graphite sheets (Russian doll model) or as a single graphite sheet rolled in around itself (parchment model) and as onion-like structure may allow the local pressure during friction to be accommodated without strong damage. Nevertheless, differences are noted between fluorinated GCBs and CNFs. The 0D GCBs exhibit friction coefficients at least equal and most of the times lower. The spherical shape of GCBs without edges could act on the friction properties. Raman analyses reveal that the friction process induces a partial deterioration of the carbon fibres, and SEM studies show the fibrous nature of the tribofilm inducing that individual carbon nanofibres play a role in the friction reduction process [12]. On the basis of those experimental facts, the properties of both CNFs and GCBs will be discussed. On one hand, fluorination of nanocarbons results in a lowering of the interparticle interactions by the reduction of the surface free energy. Fluorination of the first external layers allows such effect in the cases of CNFs and GCBs. Above the fluorination level of F/C = 0.15, the nanoparticle interaction stabilizes, resulting in friction coefficients independent on the fluorination rate in both cases. The $CF_{0.15}$ composition corresponds to a shell constituted of some tens of perfluorinated external layers for CNFs (thickness of the perfluorinated shell $\approx$ 15–20 nm).

Both peeling of some fluorinated graphene layers and decrease of the interparticle interaction could occur for nanofibres and graphitized carbon blacks. Another effect must be evoked to explain the differences between tubular and spherical shapes. SEM observation of the tribofilm formed with nanofibres revealed a thickness of 1 μm and a continuous surface which exhibits ondulations parallel to the sliding direction (Fig. 6b). Their sizes are of the same order than fluorinated fibres diameters [12,13]. An orientation of the fibres occurred during the formation of the tribofilm. In the same way, fluorinated GCBs could disaggregate and easily form a dense tribofilm, as seen by the SEM image (Fig. 6a). The thickness of the film is of 0.6 μm. The friction properties differ for GCBs and CNFs probably according to the nature of the tribofilm and suggest different friction mechanisms involving surface effects for the case of CNFs and bulk effects for the case of CNDs.

Once again, nanodiscs appear as a particular case. Very smooth aspect is observed in the high pressure zone whereas the discs are oriented parallel to the sliding direction in the low contact pressure zone (Fig. 6c). The tribofilm is mainly amorphous with some individual discs embedded in the disordered phase. Such disorganization in the high pressure zone could be a consequence of severe cleavage of the discs. For this case also, bulk effects seem to be at the origin of the friction reduction mechanism.

4. Conclusion

After the investigation of the physical–chemical properties of fluorinated 0D, 1D and 2D nanocarbons, namely graphitized carbon blacks, nanofibres and nanodiscs, which underlines similar covalent C–F bonding and closed structure, their tribological properties were investigated as a function of the fluorination levels. Whatever the fluorination level, the nanocarbons exhibit good tribological properties and can be excellent precursors for tribo-active phase in lubrication. Indeed the friction coefficients of the fluorinated nanocarbons ranged between 0.065 and 0.085, are weaker than those of most solid lubricants (graphite). An influence of the shape factor of fluorinated nanocarbons on the tribological properties is observed. Accommodation of fluorine atoms into the carbon lattice with F/C higher than 0.15 results in easy cleavage for the cases of GCBs and CNFs. The situation is different for nanodiscs because no improvement of the friction coefficient is noted after fluorination. This could be attributed to the excellent tribological properties of the non-fluorinated initial compound resulting both to extended oriented graphitic domains and shape factor. The role of fluorine atoms in cleavage is probably involved in the formation of the tribofilm. The best results are obtained for fluorinated GCBs however the shape factor of the others nanocarbons can be relevant for dispersion purpose. The difference in favour of fluorinated GCBs could appear during the formation of the tribofilm because of easy disaggregation of the spherical shape carbon blacks. Denser tribofilm may be formed using GCBs when compared to nanofibres.

References

[1] L. Joly-Pottuz, N. Ohmae, in: J.-M. Martin, N. Ohmae (Eds.), Nanolubricants, Tribology Series, 2008.
[2] F.P. Bowden, Research 3 (1950) 383–384.
[3] D. Ugarte, Nature 359 (1992) 707–709.
[4] R.F. Deacon, J.F. Goodman, Proceedings of the Royal Society of London Series A 243 (1958) 464–482.
[5] P.D. Fleishauer, J.R. Lince, P.A. Bertrand, R. Bauer, Langmuir 5 (1989) 1009–1015.
[6] J.K. Lancaster, Tribology International 23 (1990) 371–389.
[7] H. Zaidi, H. Nery, D. Paulmier, Applied Surface Science 70–71 (1993) 180–185.
[8] B.K. Yen, Wear 192 (1996) 208–215.
[9] F. Robert, D. Paulmier, H. Zaïdi, E. Schouller, Wear 687 (1995) 181–183.
[10] P. Thomas, K. Delbé, D. Himmel, J.-L. Mansot, F. Cadoré, K. Guérin, M. Dubois, C. Delabarre, A. Hamwi, Journal of Physics and Chemistry of Solids 67 (2006) 1095–1099.
[11] K. Delbé, P. Thomas, D. Himmel, J.L. Mansot, M. Dubois, K. Guérin, C. Delabarre, A. Hamwi, Tribology Letters 37 (2009) 31–41.
[12] P. Thomas, D. Himmel, J.L. Mansot, M. Dubois, K. Guérin, W. Zhang, A. Hamwi, Tribology Letters 34 (2009) 49–59.
[13] P. Thomas, D. Himmel, J.-L. Mansot, W. Zhang, M. Dubois, K. Guérin, A. Hamwi, Tribology Letters 41 (2011) 353–362.
[14] T. Nakajima, N. Watanabe, Graphite Fluorides and Carbon-fluorite Compounds, CRC press, Boston, 1991.
[15] Y. Sato, K. Itoh, R. Hagiwara, T. Fukunaga, Y. Ito, Carbon 42 (15) (2004) 3243.
[16] J. Giraudet, M. Dubois, K. Guérin, C. Delabarre, A. Hamwi, F. Masin, Journal of Physical Chemistry B 111 (51) (2007) 14143–14151.
[17] O. Ruff, O. Breitschneider, E. Ebert, Zeitschrift fur Anorganische und Allgemeine Chemie 217 (1934) 1.
[18] W. Rudorff, G. Rudorff, Zeitschrift fur Anorganische und Allgemeine Chemie 293 (1947) 281.
[19] W. Zhang, M. Dubois, K. Guérin, P. Bonnet, H. Kharbache, F. Masin, A.P. Kharitonov, A. Hamwi, Physical Chemistry Chemical Physics 12 (2010) 1388–1398.
[20] A.M. Kannan, A. Meghal, I.V. Barsukov, Electrochemistry Communications 8 (2006) 887–891.
[21] S.N. Naess, A. Elgsaeter, G. Helgesen, K.D. Knudsen, Science and Technology of Advanced Materials 10 (2009) 065002.
[22] W. Zhang, M. Dubois, K. Guérin, P. Bonnet, E. Petit, N. Delpuech, D. Albertini, F. Masin, A. Hamwi, Carbon 47 (2009) 2763–2775.
[23] S. Lynum, J. Hugdhal, K. Hox, R. Hildrum, M. Nordvik, Production of micro domain particles by use of a plasma process, patent EP1017622.
[24] F. Chamssedine, M. Dubois, K. Guérin, J. Giraudet, F. Masin, D.A. Ivanov, L. Vidal, R. Yazami, A. Hamwi, Chemistry of Materials 19 (2007) 161–172.
[25] W. Zhang, M. Dubois, K. Guérin, A. Hamwi, J. Giraudet, F. Masin, Journal of Solid State Chemistry 181 (2008) 1915–1924.
[26] A.M. Panich, Synthetic Metals 100 (2) (1999) 169–185.
[27] M. Dubois, J. Giraudet, K. Guérin, A. Hamwi, Z. FawalL, P. Pirotte, F. Masin, Journal of Physical Chemistry B 110 (24) (2006) 11800–11808.
[28] A.M. Rao, A.W.P. Fung, S.L. Di Vittorio, M.S. Dresselhaus, G. Dresselhaus, M. Endo, K. Oshida, T. Nakajima, Physical Review B 45 (1992) 688–6892.
[29] V. Gupta, T. Nakajima, B. Zemva, Journal of Fluorine Chemistry 120 (2003) 143–150.
[30] F. Withers, M. Dubois, A.K. Savchenko, Physical Review B (2010) 073403.
[31] F. Tuinstra, J.L. Koenig, Journal of Chemical Physics 53 (3) (1970) 1126–1130.